Proceedings of ASME Turbo Expo 2011
GT2011
June 6-10, 2011, Vancouver, British Columbia, Canada

GT2011-45860

APPLICATION OF AN INVERSE CASCADE ANALYTICAL AND NUMERICAL DESIGN METHOD USED IN THE DESIGN OF AXIAL FANS

Mihai Miclea-Bleiziffer, Philipp Epple, Henrik Smith, Matthias Semel and Antonio Delgado
Institute of Fluid Mechanics, LSTM
Friedrich-Alexander University, Erlangen-Nuremberg,
Cauerstrasse 4, 91058 Erlangen, Germany
Tel: +4991318529485
Fax: +4991318529503
Corresponding author: mihai.miclea@lstm.uni-erlangen.de

ABSTRACT

This contribution presents an inverse design method for axial flow fans validated by 3-D RANS numerical simulations. It is based on an analytical performance derivation for different free-vortex distributions combined with a mean-line pre-design tool and supported by a new 2-D cascade potential flow computational method. This computes the 2-D planar cascade flow field and the inviscid deflection angle of thin arbitrary shape airfoils at different machine radii followed by a numerical radial integration into a quasi-3-D method. For validation, several fan designs were investigated, showing the influence of important design parameters as well as the potential of the present method by redrafting an industrial fan. The 2-D planar potential cascade code was validated against the Weinig's coefficient diagram for flat plate and circular arc cascades.

INTRODUCTION

The design of axial fans is investigated by using non profiled thin cambered airfoils as firstly mentioned in Eck [6]. A new inviscid 2-D cascade computational approach is used so that no predefined airfoil data are needed. The workflow is outlined in Figure 1. The 2-D inviscid deviation angle is predicted by means of new inviscid cascade computation approach using a potential core instead of the cascade loss model as previously done in references [21], [24], [25]. The methods would lose their validity for the airfoil shapes investigated here, as well as the approach of Wallis [23]. The new procedure was successfully validated against Weining's coefficient diagram as a function of cascade solidity [5]. Various vortex distributions are often recommended ([1], [10], [23], [24]) but without an analytical analysis of their impact on performance envelope. This contribution shows analytically how the free-vortex distribution can be specified at any desired flow-rate and how this influences the performance envelope of axial fans. As shown in Figure 1, the first step of this approach isolates the design requirements based on measurements or CFD results. The vortex-distribution and the blade angle are then specified according to the analytical framework. With these, a mean-line is chosen. Next, a quasi-3-D potential-flow analysis is performed with the resulted blade design to capture the exit angle deviations. The resulting geometry is then evaluated by numerical RANS 3-D simulations.

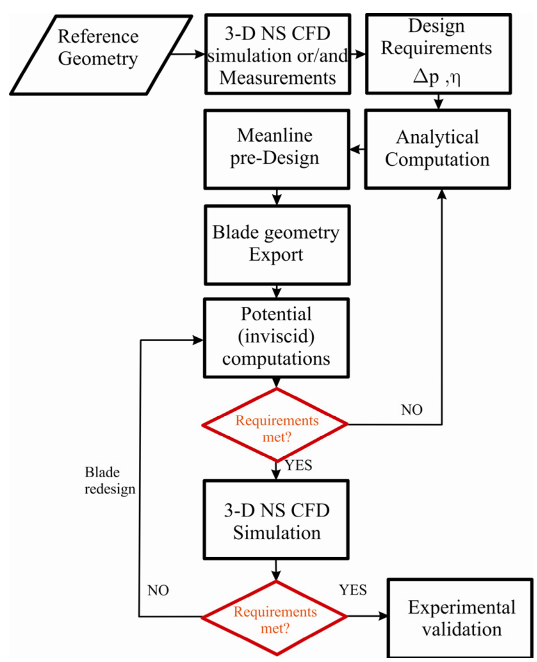

Figure 1 SCHEMATIC FAN DESIGN PROCEDURE

If the design requirements are not met in any of the previous steps, the number and/or shape of the blade elements will be optimized iteratively. The final validation of the geometries occurs experimentally. A truck cooling fan was optimized with this proposed method. The experimental validation of the optimized fan is in process. The result will be presented in a separate paper.

ANALYTICAL PERFORMACE DERIVATION FOR AXIAL FANS

A typical cascade is obtained by projecting a cylindrical meridional stream surface at a radius r, in Cartesian coordinates. For an axial fan we can make the following simplification before deriving the fundamental equations:

- No pre-swirl condition according to [1] as depicted in Figure 2:
  $$c_{u1} = 0 \Rightarrow c_1 = c_{m1}$$
- The meridional component of the velocity (mass flow component) is equal at inlet and at outlet (Figure 2):
  $$c_1 = c_{m1} = c_{m2}$$
- The flow at the inlet is shock-less
- The flow is blade-congruent.

For the section of a simple stage axial fan, the Euler equation in the total-pressure form reads:

$$\Delta p_{t12} = \frac{\rho}{2}\left[\underbrace{\left(w_1^2 - w_2^2\right)}_{\substack{static\\component}} + \underbrace{\left(c_2^2 - c_1^2\right)}_{\substack{dynamic\\component}}\right] \quad (1)$$

Static pressure can be transformed using the properties of the velocity triangles to the following expression:

$$\Delta p_{s12} = \frac{\rho}{2}\left(U^2 - c_1^2 \tan^2\left(\beta_2\right)\right) \quad (2)$$

The total pressure Δp_t from eq. 1 can be reduced to the following form:

$$\Delta p_{t12} = \rho U c_{u2} \quad (3)$$

Further it can be expressed as a function of the outlet angle:

$$\Delta p_{t12} = \rho U \left(U - c_1 \tan\left(\beta_2\right)\right) \quad (4)$$

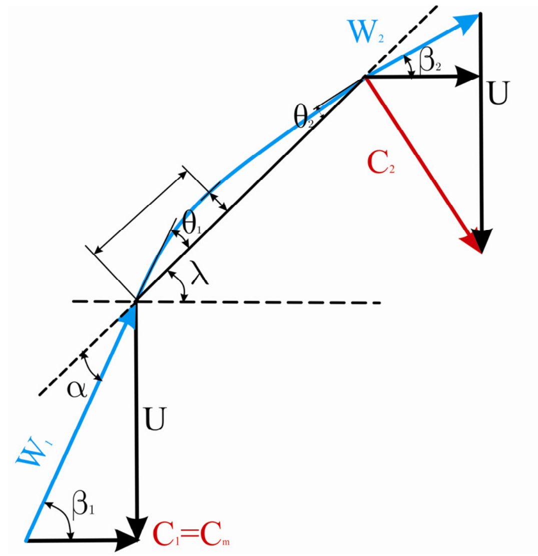

Figure 2 CASCADE WITH INLET AND OUTLET VELOCITY TRIANGLES ACCORDING TO THE MEAN-LINE THEORY

The total-to-static pressure ([7],[8],[11]) can be written according to [9] :

$$\Delta p_{t-s} = \Delta p_{s12} - \frac{\rho}{2} c_1^2 = \Delta p_t - \frac{\rho}{2} c_2^2 \quad (5)$$

(For the sake of brevity the use of indices (1-2) for defining the stage is dropped from further use.) Eq.5 can be further expressed as:

$$\Delta p_{t-s} = \frac{\rho}{2}\left(U^2 - c_1^2 \tan^2\left(\beta_2\right)\right) - \frac{\rho}{2} c_1^2 \quad (6)$$

In a recent study [9] the author has shown that this is the relevant pressure when designing axial fans. However, this is not always appropriate as for example, when a stator is present after the rotor, which recovers the dynamic head of the swirl. Many definitions for the efficiency of turbomachines can be found in literature, as stated in Dixon [21]. Therefore it is sometimes difficult to choose the proper one for a specific application.

Given the ideal case, the total hydraulic power transmitted to the shaft is equal to the power of the shaft. Therefore the required shaft energy can be written as the product of total pressure and the flow-rate. However, if the total-to-total pressure efficiency is evaluated based on the previously derived equations, this will always be equal to 1. In the case of a total-to-static pressure the *"total-to-static efficiency"* can be defined [9]:

$$\eta_{t-s} = \frac{\Delta p_{t-s} Q}{\Delta p_t Q} = \frac{\Delta p_{t-s}}{\Delta p_t} \quad (7)$$

Substituting the expression for Δp_{t-s} (eq.7) and Δp_t (eq.5), η_{t-s} is transformed in the fallowing expression:

$$\eta_{t-s} = \frac{1}{2}\frac{\left[\left(U - \frac{c_1^2}{U}\left(\tan^2\left(\beta_2\right)+1\right)\right)\right]}{\left(U - c_1\tan\left(\beta_2\right)\right)} \tag{8}$$

It was shown in [9] that the reaction is not a proper performance parameter for design. The total-to-static efficiency η_{t-s} was used instead.

Until this point, the derivation has been done only for one cylindrical meridional section of the axial machine. Since geometrical characteristics of blade sections change as one moves from hub to tip, their variation on the global design has to be considered. At the beginning of the derivation one has to assume a radial vortex distribution. Two types of vortex-distributions are distinguished based upon radial equilibrium [1], [3]. We assume the free-vortex distribution in the further analysis. Based on the angular momentum equation this condition reads:

$$c_{u2}\, r = const \tag{9}$$

This means that every radial section of the fan will have the same total pressure increase since the peripheral component of the absolute velocity c_{u2} together with the peripheral velocity are the only parameters in the total-to-total pressure equation (eq. 3). The free vortex design-point can be adjusted at *any desired flow-rate* as pointed by the radial β_2 distribution:

$$\beta_2\left(r\right) = \arctan\left(\frac{2\cdot\pi\cdot r\cdot n - k\left(2\cdot\pi\cdot r_h\cdot n - c_{md}\cdot\tan\left(\beta_{2h}\right)\right)}{c_{md}}\right) \tag{10}$$

Whereas c_{md} is the free-vortex-design-velocity is expressed upon the free-vortex-flow-rate (Q_d):

$$c_{md} = \frac{Q_d}{\pi\left(r_t^2 - r_h^2\right)} \tag{11}$$

Miclea et al. [9] showed that the integral expressions for the static pressure, total pressure and total-to-static pressure are:

Static pressure

$$\Delta p_s = \frac{\rho}{A}\int_{r_h}^{r_t}\left[U_r^{\,2} - \left[c_1\frac{\left[U_r - k\left(U_h - c_{md}\tan\left(\beta_{2h}\right)\right)\right]}{c_{md}}\right]^2\right]\pi\, rdr \tag{12}$$

Total pressure

$$\Delta p_t = \frac{\rho}{A}\int_{r_h}^{r_t}U_r\left[U_r - c_1\frac{\left[U_r - k\left(U_h - c_{md}\tan\left(\beta_{2h}\right)\right)\right]}{c_{md}}\right]2\pi\, rdr \tag{13}$$

Total-to-static pressure

$$\Delta p_{t-s} = \frac{\rho}{A}\int_{r_h}^{r_t}\left[U_r^{\,2} - \left[c_1\frac{\left[U_r - k\left(U_h - c_{md}\tan\left(\beta_{2h}\right)\right)\right]}{c_{md}}\right]^2 - c_1^{\,2}\right]\pi\, rdr \tag{14}$$

The total-to-static efficiency can be written as the ratio between the total-to-static and total pressure given by the last integral equations.

For the investigated case in this contribution, a performance analysis is performed aiming a consistent improvement of the total-to-static efficiency by keeping at least the same pressure characteristics at the operating point. The performances (computed as described in the CFD setup section) and geometric dimensions of the reference fan are depicted in Table 1. The maximum tip radius r_t was fixed in this study as a design constraint. It originates from the reference fan.

The performance impact of two design parameters was investigated: the free-vortex design-flow-rate (Q_d) and of the outlet-hub-angle (β_{2h}). This can be achieved by changing one of the parameters while keeping the other constant as it will be shown in the study given in the next section. After finding an optimum value for one of the design parameters, its value will be fixed and the procedure will be iterated by changing the other design parameters until is found an optimum value for each of them.

PARAMETER	VALUE	UNITS
r_t	0.28	[m]
r_h	0.143	[m]
k	0.51	[-]
U	3000	[rpm]
Q_D	4	[m^3s^{-1}]
$\Delta p_{t-s}\ at\ Q_D(CFD)$	1500	[Pa]
$\eta p_{t-s}\ at\ Q_D(CFD)$	0.49	[-]
z	8	[-]

Table 1 GEOMETRICAL AND CFD PERFORMANCE PARAMETERS OF THE REFERENCE IMPELLER

POTENTIAL BLADE ANALYSIS

1. Description of the plane 2-D cascade model

In the previous section, the one-dimensional mean-line based analysis was exposed. An extension of this theory can be achieved by analyzing the two-dimensional flow in a cascade of thin cambered airfoils. For achieving this, a new method was developed using the potential-flow theory.

The aerodynamic analysis problem of airfoils is solved in many classic textbooks by dividing it in two main influences: the camber influence and the thickness influence as depicted for instance in Figure 3.

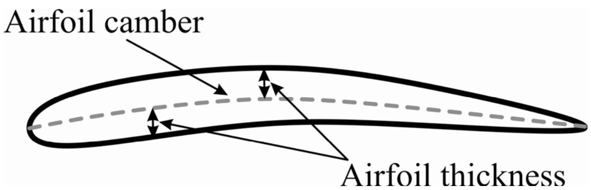

Figure 3 CAMBERED AIRFOIL

The method of handling the two-dimensional flows in turbomachinery cascades is described in Lewis [1] and has originally been developed by Martensen [2]. Lewis [1] solves the complex potential problem for two-dimensional cascade numerically, by using a vortex panel distribution. However, this method has been developed for thick airfoils. It solves both the camber and the thickness distribution problem. Previously to Martenesen, Weinig [4] has solved analytically the complex potential problem of straight two-dimensional cascades [4]. Later, he developed a method of solving the exact potential flow through the cascades of circular arcs. However, none of these methods could solve the problem for cascades of arbitrary shape [11]. Lakshminarayana [11] reports the Weinig-analysis of camber-lines as unpractical for design purposes. Schlichting and Scholz have published a paper [22] showing how this could be handled with the classical vortex distribution approach of Birnbaum for the cascades of a compressor. The problem can be solved numerically in a different manner than previously by Schlichting [22] by deriving a vortex panel method for an infinite array of thin-foils. In the framework of vortex panel methods the complex potential of a cascade reads [1]:

$$u - iv = \frac{i\Gamma}{2t}\cosh\left(\frac{z}{2}\right) = \frac{i\Gamma}{2t}\left(\frac{\sinh(x) - i\sin(y)}{\cosh(x) - \cos(y)}\right) \quad (15)$$

The velocity induced by a vortex of circulation Γ at (x_0,y_0) at an arbitrary point of coordinates (x, y) reads [3]:

$$u = \frac{\Gamma}{2\pi}\frac{(y-y_0)}{(x-x_0)^2+(y-y_0)^2} \quad (16)$$

$$v = \frac{-\Gamma}{2\pi}\frac{(x-x_0)}{(x-x_0)^2+(y-y_0)^2} \quad (17)$$

The normal vector on a surface panel reads:

$$n = \left(\sin(\zeta), \cos(\zeta)\right) \quad (18)$$

So that the influence coefficients are computed according to:

$$a = (u,v)\cdot n \quad (19)$$

And the RHS reads [3]:

$$RHS = -V_{\inf}\left[\cos(\alpha)\sin(\zeta) + \sin(\alpha)\cos(\zeta)\right] \quad (20)$$

The strengths of the panel vortex:

$$\Gamma = [a][RHS]^{-1} \quad (21)$$

For the computation of an airfoil row eq. 16 and 17 were adapted in eq.15 and after some manipulations we obtain:

$$u_{cascade} = \frac{\sin(a)\left(-\sin(\lambda+\zeta)\right)}{2t\left(\cosh(b) - \cos(a)\right)} \quad (22)$$

$$v_{cascade} = \frac{-\sinh(b)\left(\cos(\lambda+\zeta)\right)}{2t\left(\cosh(b) - \cos(a)\right)} \quad (23)$$

With λ as stagger angle (Figure 4) , and a and b are defined as:

$$a = \frac{(y-y_0)\cos(\lambda) + (x-x_0)\sin(\lambda)}{2\pi t} \quad (24)$$

$$b = \frac{(x-x_0)\cos(\lambda) - (y-y_0)\sin(\lambda)}{2\pi t} \quad (25)$$

The influence matrix:

$$A_{cascade} = u_{cascade} + v_{cascade} \quad (26)$$

With the RHS of the cascade written in matrix form:

$$RHS_{cascade} = -V_{\inf}\begin{bmatrix}-1 & 1\end{bmatrix}\begin{bmatrix}\cos(\alpha+\lambda)\sin(\zeta+\lambda)\\ \sin(\alpha+\lambda)\cos(\zeta+\lambda)\end{bmatrix} \quad (27)$$

It yields to the solution for the airfoil vortex strength:

$$\Gamma_{cascade} = \left[A_{cascade}\right]\left[RHS_{cascade}\right]^{-1} \quad (28)$$

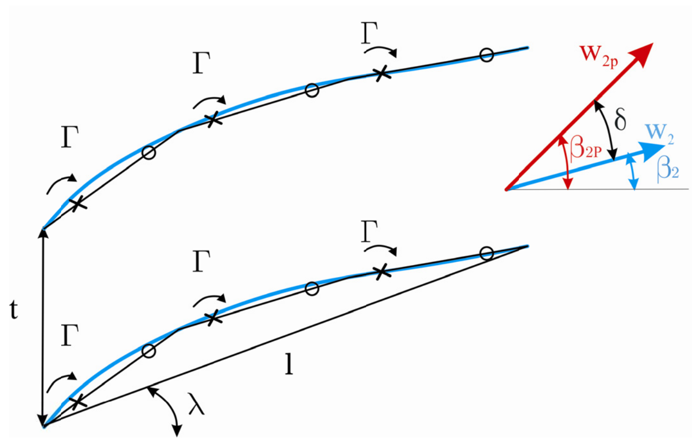

Figure 4 CASCADE OF THIN AIRFOILS WITH FIGURED VORTICES AND DEVIATION ANGLE

By solving the above system for a sufficient number of points, the vortex distribution on the camber-line will be obtained. From the vortex distribution one can compute the velocity distribution over the blade and the desired velocity and pressure field around the cascades. The two-dimensional solution can compute the velocity distribution and thus the inviscid flow angle β_{2P} at the cascade exit. As from equations 2, 4, and 5 this plays the key role for the turbomachine performances. The deviation angle δ represents in this case the two-dimensional cascade loss as depicted in Figure 4. Figure 5 illustrates flow streamlines of a camber-line cascade computed by the present method for pointing out the difference between blade angle and flow-angle. The validity of the proposed method is proved by representing the results of the Weinig-Coefficient computation with the present method against the

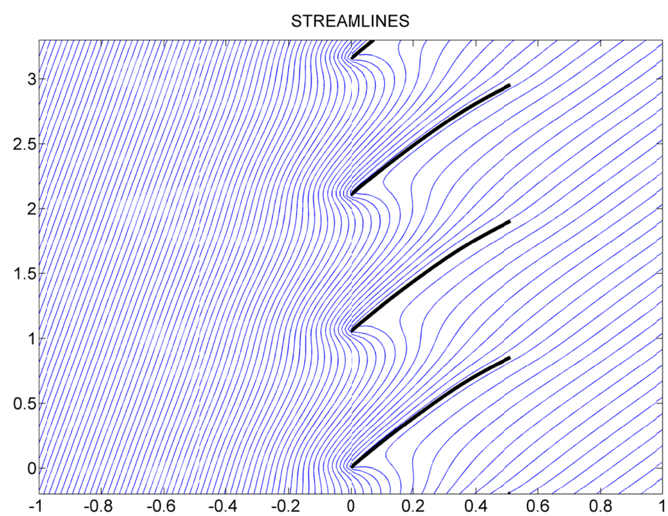

Figure 5 STREAMLINES IN A TWO-DIMENSIONAL CASCADE COMPUTED BY THE PRESENT METHOD

original Weinig-Coefficient diagram in the version presented in Scholz [5] as depicted in Figure 6. K represents the ratio between lift coefficient of the airfoil in cascade at different solidities and the lift coefficient of the same airfoil alone.

Only some of the stagger angles are illustrated in Figure 6 in order to enhance the overview. The results computed by the present method are found to be in a very good agreement to the ones published in Scholz [5].

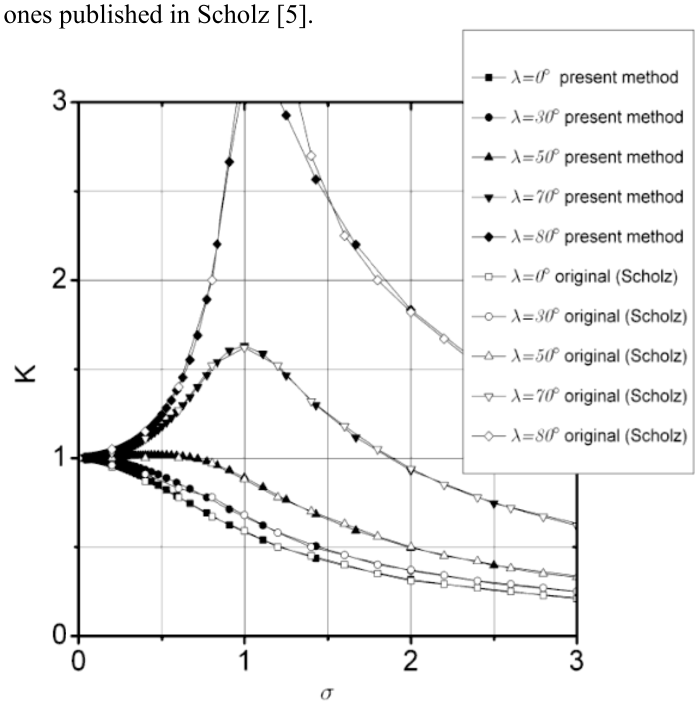

Figure 6 WEINIG'S COEFFICIENT (K) FOR FLAT PLATE CASCADES REPRESENTED AS A FUNCTION OF THE BLADE SOLIDITY

2. 2-D integrated/Quasi-3-D Method

A 2-D integrated method is used to calculate the flow in the fan quasi-three-dimensional. Therefore, the potential flow is calculated on a number of coaxial sections that are distributed over the radius of the blade. The individual results are then mass-flow average-integrated. Radial velocities and their influence are not considered in this computational framework. Thus, this method takes into account only the influence of the deviation angles at every computed radial section and their mass-flow integrated value.

The presented quasi-3-D method is used both for the calculation of design and offdesign conditions. Hereby a constant radial meridian velocity is assumed for all cases. This simplification is advantageous in the sense that it allows a pre-assessment of a large number of design options in a very short time. The designs which fall within the desired performance range are shortlisted for the full scale 3-D numerical simulations.

THE DESIGN METHOD STEPS

1. Mean-line blade generation

The main assumptions for the predesign blade generation process are that the flow is inviscid, and one-dimensional. However, the real flow will never be like this since it is three-dimensional viscous and turbulent. Nevertheless, a good blade shape will guide the flow inside the channel in such a way that the losses will be minimal and it will achieve performances very close to the desired ones. The core of blade-generation process, in the assumptions stated previously is the matching method between the inlet and outlet angles, which are received as an input from the analytical analysis. The coupling of the blade angles is made as depicted in Figure 7 by inserting two other conditions required for the definition of the cascade: the angle α and the stagger angle λ. The angle α is defined as the angle between the relative inflow velocity and the stagger angle (Figure 7). As already mentioned, the sections of the blades will be designed with very thin airfoils. Figure 7 depicts a thin airfoil from a cascade showing a correlation between the inlet and outlet flow angles, blade cambers and stagger.

The inflow angle with the no swirl condition at the design flow-rate ($Q_d = 100\%$) (axial entry) reads:

$$\tan(\beta_1) = \frac{U_{section}}{c_1} \tag{29}$$

From the geometry of the thin airfoil the inlet and outlet camber angle can be geometrically derived:

$$\tan(\theta_1) = \frac{dy}{dx} \tag{30}$$

$$\tan(\theta_2) = \frac{dy}{dx} \tag{31}$$

Further based on Figure 7 the inlet flow angle can be derived for a shock-less entry in the cascade:

$$\beta_1 = \theta_1 + \lambda \tag{32}$$

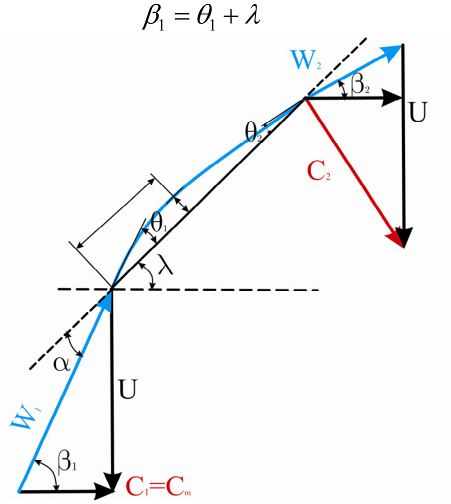

Figure 7 INLET AND OUTLET BLADE ANGLES

The cascade stagger angle is expressed:

$$\lambda = \beta_1 - \alpha \tag{33}$$

The outlet flow angle is geometrically obtained:

$$\theta_2 = \lambda - \beta_2 \tag{34}$$

For solving the system of equations (eq. 32, 33, 34), λ can be eliminated from the first two relations and a first relation can be determined between alpha and the inlet camber:

$$\theta_1 = \alpha$$

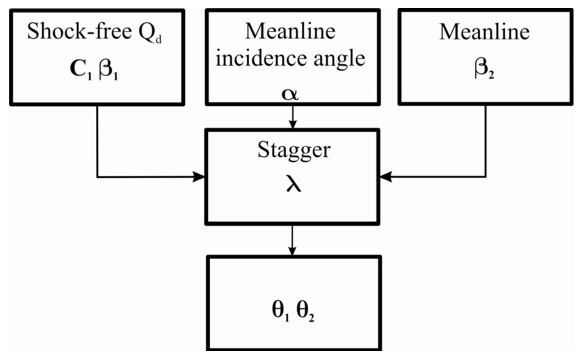

Figure 8 WORKFLOW DIAGRAM OF THE MEAN-LINE BLADE GENERATION PROCESS

The angle distribution between inlet and outlet is given by a function. In this contribution we used a NACA 4 Digit function but this represents no limitation, the method can be used for any arbitrary function. The camber and camber position of a NACA-4 Digit camber-line are determined when solving the following equation system. Angle α is still unknown, but for any value of it the stagger angle λ and the inlet and outlet camber are known and so are the camber and camber position (m,p in eq. 35 and 36) required for the NACA function. All these relations and the workflow are shown in Figure 8.

$$y_2 = \frac{m}{p^2}\left[2\,p\,x_2 - (x_2)^2\right] \tag{35}$$

$$y_{n-1} = \frac{m}{(1-p)^2}\left[(1-2\,p) + 2\,p\,x_{n-1} - (x_{n-1})^2\right] \tag{36}$$

The blade section generating process is repeated for every radial section. The radial inlet angle distribution is given by eq. 29 while the exit angle distribution is computed by eq. 10 which is developed by further equating of eq. 9. Once the hub exit angle β_{2h} and the desired free-vortex-flow-rate are set, the radial distribution of exit angle $\beta_2(r)$ is computed and therefore all blade sections can be defined.

An example of stacked blade sections is illustrated in Figure 9. Here the sections are stacked at 25% of the chord. The pitch-chord-ratio respectively the number of blades has not been set yet. Prior to finding the optimum number of blades, an overview of the main blade influence parameters and of the inviscid deviation angle on the performances of axial fans is given in the next sections of the present study.

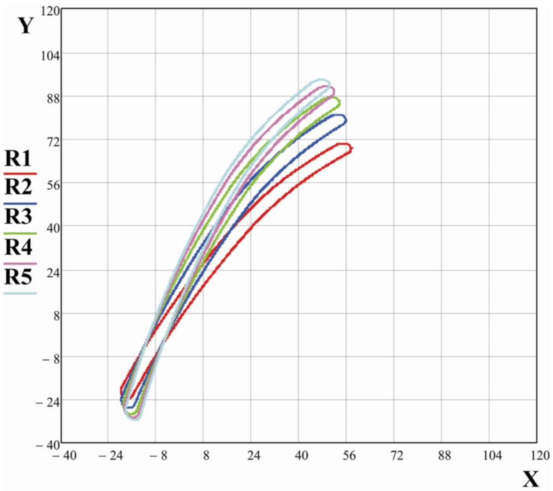

Figure 9 Stacked radial blade sections in the x,y cascade plane

2. Theoretical and quasi three-dimensional performances for an example axial fan

In this section the analytical performances in terms of total-to-static pressure and total-to-static efficiency are presented starting with a variation of the design flow-rate for the free-vortex design and a variation of the exit blade angle while keeping the same inlet angle β_1 designed for the flow rate Q_d=100%. A mass flow-averaged exit-angle was computed for each designed section by using the plane two-dimensional computation. This is introduced in the analytical equations in the first section, and the loss due to the two-dimensional flow in terms of Δp_{t-s} and η_{t-s} is obtained. These results are compared with the one-dimensional analytical solution in this section. The quasi-3-D computations used the same blade spacing for all investigated cases.

In Figure 10 the influence of the free-vortex design point is presented while keeping β_{2h} constant at a value of 45°. The design parameter Q_d is fixed at 4 flow-rates from 4 m^3/s (100% of the desired working point) to 24 m^3/s (600% of the desired working point). The tendency is clearly indicated on the different Q_d pressure-slopes: the higher the design-flow-rate for the free-vortex condition the higher is the achievable flow-rate. The value of the maximum Δp_{t-s} stays the same at zero flow-rate since it is independent of the design-flow-rate as given by eq. 14. From the analytical point of view the tendency shown in Figure 10 means that the maximum achievable flow-rate and the total-to-static-pressure slope can be influenced only by the free-vortex-design-flow-rate Q_d.

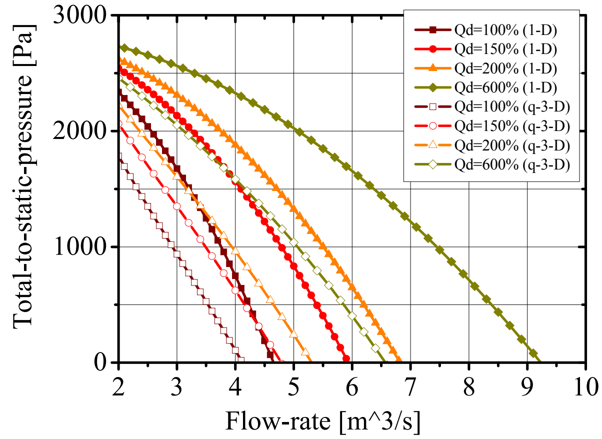

Figure 10 ANALYTICAL AND QUASI-3D TOTAL-TO-STATIC PRESSURE OF THE FAN FOR DIFFERENT FREE-VORTEX MERIDIONAL DESIGN FLOW-RATES

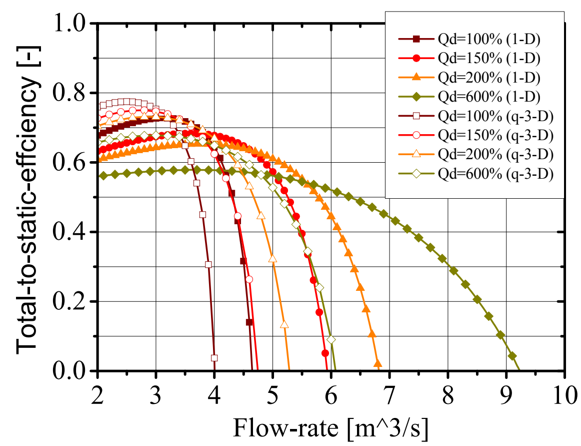

Figure 11 Analytical and Quasi-3D total-to-static efficiency of the fan for different free-vortex meridional design velocities

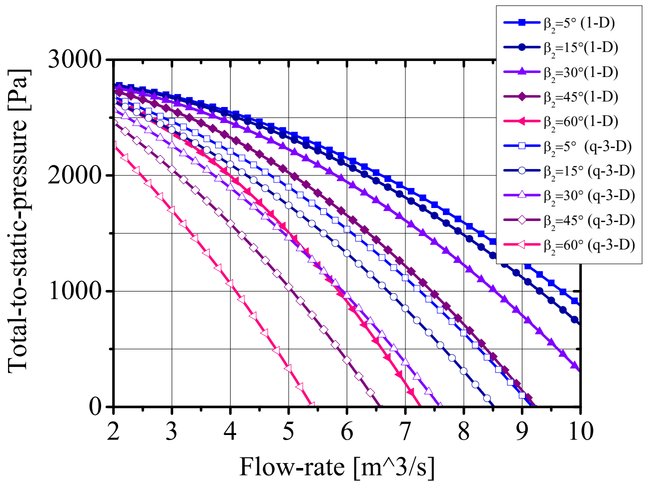

Figure 12 Analytical and Quasi-3D total-to-static pressure of the fan for different hub blade angles

The results of the potential computation show a loss of the designed pressure for all the designs. This is due of the angle deviation (Figure 4). The total-to-static efficiency tendency indicates this is higher, and reaches its maximum η_{t-s} while the design flow-rate is lower as depicted in Figure 11. The effect of the quasi-3-D computation on the total-to-static efficiency η_{t-s} shows it increases while the maximum flow-rate decreases. As a result of the deviation angle, β_2 increases in and so does the total-to-static efficiency η_{t-s} (eq. 8).

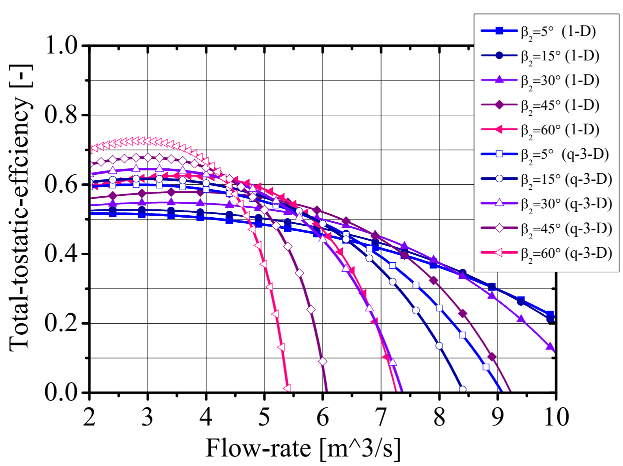

Figure 13 ANALYTICAL AND QUASI-3D TOTAL-TO-STATIC EFFICIENCY OF THE FAN FOR DIFFERENT HUB BLADE ANGLES

The analytical dependence of Δp_{t-s} in axial fans on the exit angle β_2 prescribed at the hub section is presented in Figure 12. For computing the Δp_{t-s} and η_{t-s} characteristics, the free-vortex-design flow-rate Q_d was kept constant at the value of 24 [m^3/s] (600% of the desired working point). When decreasing the angle down towards 0° the maximum achievable flow rate for the static pressure Δp_{t-s} increases considerably.

The highest efficiency is obtained when designing with high outlet angles, but the machine works at smaller flow-rates as depicted in Figure 13. Since the flow exit angle gets higher in the quasi-three-dimensional case the efficiency will increase when compared to the one-dimensional theory.

The results of the potential computation show a loss of the designed pressure for all the designed fans. Previously it was shown by the authors [9] that the peak pressure at zero flow-rate is not depending upon any other factor then the peripheral velocity.

3. 3-D CFD setup

The simulation setup for the 3-D RANS CFD is shown in Figure 14. References about pipe test-rig measurements of axial fans are available in Wallis [23], Eck [6] or Eckert [12] . The CFD model was divided in 3 computational domains: the inlet domain, the fan domain (rotating) and the outlet domain (Figure 14).

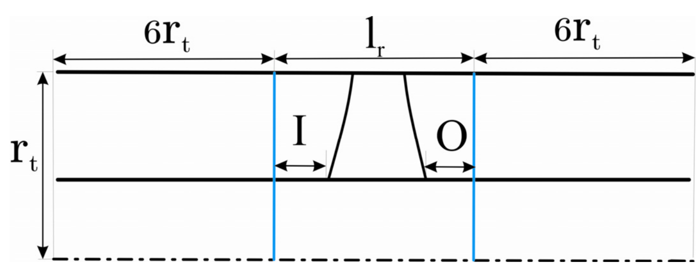

Figure 14 SIMULATION SETUP STARTING FROM LEFT: INLET, FAN AND OUTLET

The fan was generated without the gap between tip and housing in order to reduce the number of nodes and computational effort. The main dimensions of the flow field are depicted in Table 2. Numerical simulations were performed on high performance computers (HPC) with ANSYS CFX® 12.1. Around 7 steady-state simulations were carried out for the reference fan for and each of the new designs by changing the flow rate from 2 to 8 [m^3/s]. For the investigated case (aerodynamic flow) Bardina et al. [15] showed that the Shear Stress Turbulence model (SST) of Menter [14] has the best overall results. Also in Hirsch [20] the SST model shows the best predicting capability for a diffuser-case when compared to other turbulence models. The adaptive wall functions implemented in ANSYS-CFX® v. (12.1) were used in the simulations.

PARAMETER	VALUE
Inlet length	$6r_t$
Outlet length	$6r_t$
Interface to blade length (I)	60[mm]
Interface to blade length (O)	O>50[mm]
Rotor length (l_r)	180[mm]

Table 2 DIMENSIONS OF THE CFD FLOW FIELD

In Table 3 are shown the main settings for the simulations. The mass-flow-rate and pressure at the interfaces as well as at the inlet and outlet were monitored in the solver during the simulation. The simulations reached the convergence criteria after approximately 500 iterations and the convergence criteria were set at RMS $1e^{-4}$.

SIMULATION PARAMETER	VALUE
Inlet	mass flow [kg s^{-1}]
Inlet Turbulence	1%
Inlet Temp.	25°C
Outlet	opening static pressure 0 [Pa]
Outlet Temp.	25°C
Outlet Turbulence	5%
Walls/Blades/Hub/Casing	No slip walls
Interfaces	GGI/Frozen Rotor
Turbulence model	SST
Rotating speed	3000[rev m^{-1}]
Density	1.185[kg m^{-3}]

Table 3 SIMULATION SETUP

4. Grid generation and grid study

As stated in the previous section the computational domain used for the present study is composed from three separate parts: an inlet part, the fan domain and an outlet domain. In the books of Peric [19] and Hirsch [20] as well as in the CFX-Solver Manual [17] can be found in-detail descriptions about the correct grid treatment for computations of internal flows using two-component turbulence models. In the mentioned works the most accurate grid for CFD simulations is a hexahedral grid. For the generation of the grids in this contribution, two commercial software programs were used: ANSYS ICEM® and ANSYS TurboGrid®. The first one was used for generating the test-rig and outlet domains, while the second one for generating the fan domain. The inlet and outlet pipes have the same geometry and the same grid spacing; their grid was generated using hexahedral elements. The spacing of the grid points was distributed bi-exponentially in the radial direction for the near-wall-treatment. For increasing the accuracy of the computation in the stream-wise direction the distribution of elements was adjusted with an exponential function, so that the elements near the fan interface region became smaller, as depicted in Figure 15. The number of elements was adjusted in the radial and peripheral direction according to the grid of the blade channel.

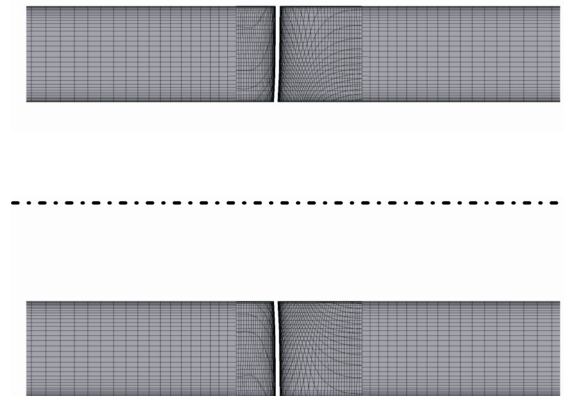

Figure 15 SECTION TROUGH INLET, FAN AND OUTLET GRIDS

The rotor grid was generated by using the turbo-machine dedicated grid generator from ANSYS, TurboGrid (Figure 16). In this software the geometry of a blade channel is automatically created based on a set of radial-spaced-airfoils, hub and shroud curves. Different grid generation options are available in the program including a full automatic grid generation by specifying the target number of elements in the blade channel. For the geometries presented in this study the grid generation was performed automatically using the ATM-beta option.

In the CFD simulations the accuracy of the computed near-wall turbulence and implicit of the high turbulent regions computations is strongly dependent from the number of grid points within the computed boundary layer and the non-dimensional grid spacing of the first element from the wall as described in Peric [19] and [17]. In ANSYS TurboGrid® this

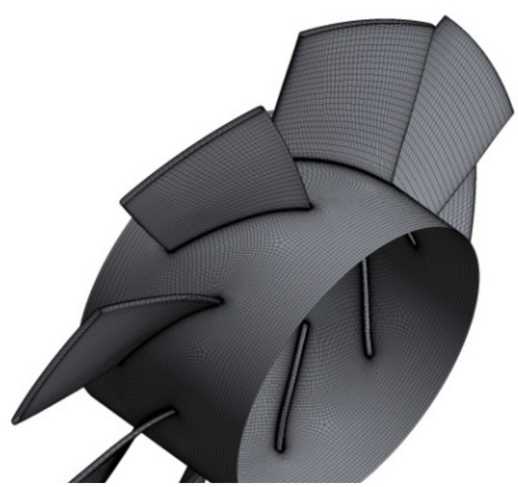

Figure 16 FAN GEOMETRY WITH MESH GENERATED IN ANSYS TURBOGRID®

can be adjusted by setting an average Re-number (radial average based on the chords lengths and relative velocity), the non-dimensional wall-spacing y+ and the wall normal height of the airfoil-surrounding O-Grid. In order to ensure the convergence of the solution and the optimal grid parameters of the studied geometries a grid study was performed for the reference fan. To ensure the convergence for all flow-rate simulation the grid study was conducted at the expected operating point and also at partial load and overload (50%flow-rate and 150%flow-rate)). Figure 17 depicts the results of the grid study for different operating points. As a result of the grid convergence study, grids with approximately 200000 elements per channel were used for the simulations in this contribution. Each of the inlet and outlet grids had 575000 elements. The complete domain had ~2760000 elements.

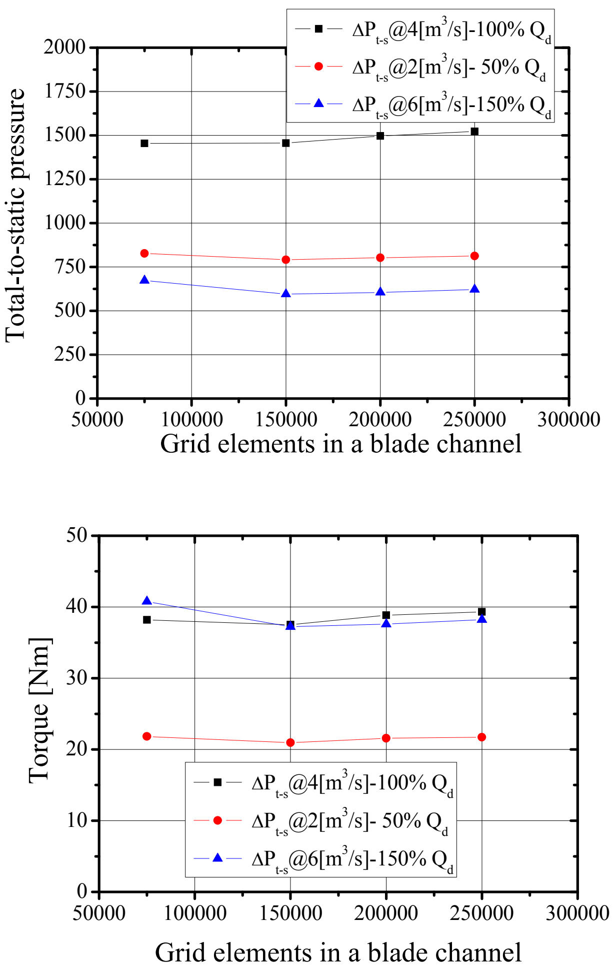

Figure 17 GRID STUDY CONVERGENCE

5. Comparison of the quasi-3-D and CFD simulations

In this section the results of the quasi-3-D approach and 3-D-RANS CFD are illustrated and discussed. In Figure 18 the free-vortex flow-rate prescription for Δp_{t-s} is investigated in the case of quasi-3-D simulations and 3-D CFD simulation. The

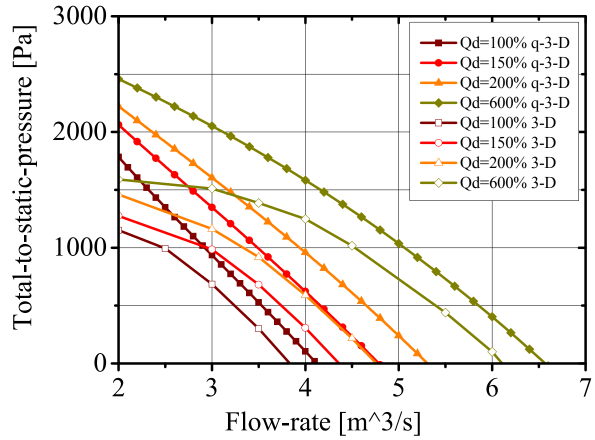

Figure 18 QUASI-3D AND FULL 3-D CFD TOTAL-TO-STATIC EFFICIENCY OF THE FAN FOR DIFFERENT FREE-VORTEX MERIDIONAL DESIGN FLOW-RATES

CFD results are in satisfactory agreement with the potential ones and they show qualitatively the same tendency. This means that the quasi-3-D predicts with reasonable accuracy the pressure behavior and the maximum flow-rate as well.

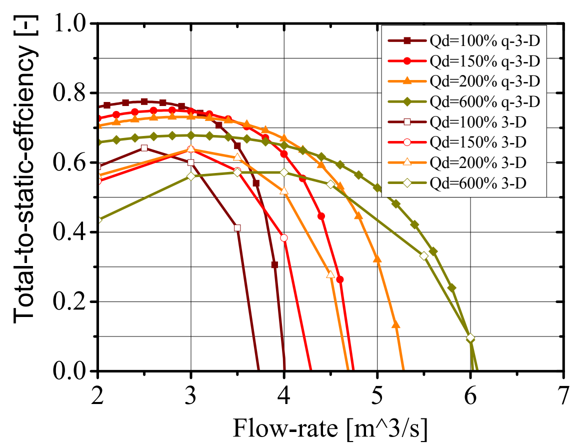

Figure 19 QUASI-3D AND FULL 3-D CFD TOTAL-TO-STATIC PRESSURE OF THE FAN FOR DIFFERENT FREE-VORTEX MERIDIONAL DESIGN FLOW-RATES

The differences between them are explained by the presence of viscosity and turbulence losses in the RANS 3-D CFD simulations. These results are relatively close to the potential ones when comparing the efficiencies η_{t-s} (Figure 19).

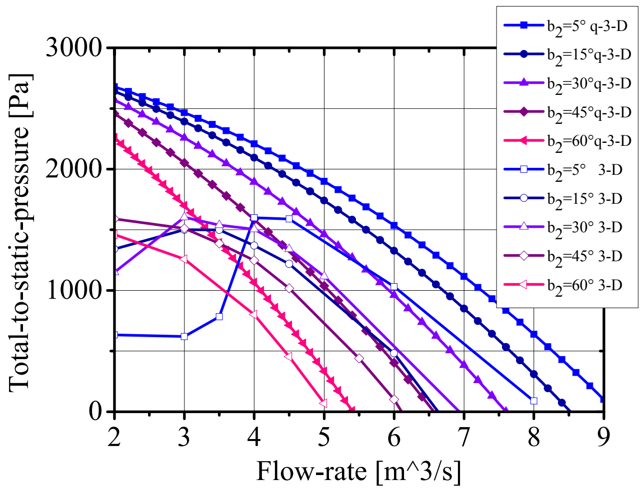

Figure 20 QUASI-3D AND FULL 3-D CFD TOTAL-TO-STATIC PRESSURE OF THE FAN FOR DIFFERENT HUB BLADE ANGLES

A boundary layer approach complementary to the potential model could predict also the friction losses and would improve the accuracy of quasi-3-D predictions. The working point flow-rate is predicted with reasonable accuracy by the potential method for all the investigated cases in Figure 19.

The same pattern of agreement is indicated in Figure 20, where the influence of the hub exit angle β_2 upon Δp_{t-s} is studied. There are two exceptions from the relative good qualitative agreement illustrated in figure: the case of the design with β_2=5° and the one with β_2=15°.

The design having a β_2=5° prescription surges bellow 4 [m^3/s],

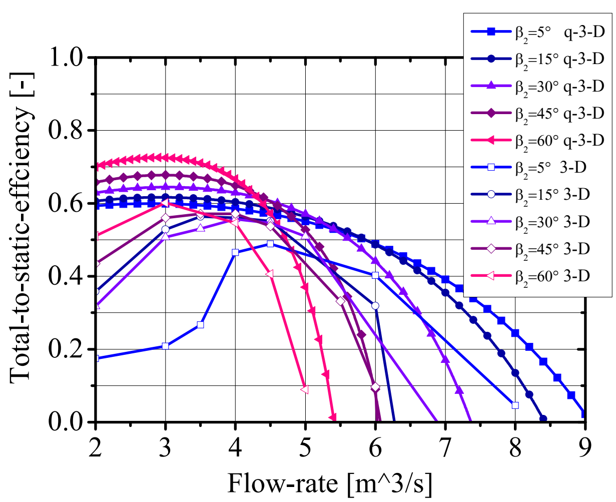

Figure 21 QUASI-3D AND FULL 3-D CFD TOTAL-TO-STATIC EFFICIENCY OF THE FAN FOR DIFFERENT HUB BLADE ANGLES

and presumably this is due to the very high turning angle ($\Delta\beta$), which cannot be fulfilled by the flow patterns at low flow-rates.

Also the β_2=15° design has a different behavior than the potential computation, its pressure increase is below the one of the β_2=30° design as depicted in Figure 20. The blade sections of this design have higher turning angle than in the other investigated designs, which could be a reason for this behavior. Hence the blades with high turning angles should be deeper analyzed in the opinion of the authors and this will be presented in a future publication. The efficiency of these designs is illustrated in Figure 21 and shows the same qualitative agreement with the potential computation as in the previous case. In the potential computation the relative efficiency difference between the investigated designs is obvious but in the CFD computation this reduces to almost zero. Differences appear in the same cases as previously discussed, for the blade designs with high turning angle: β_2=5° and β_2=15°.However, the blade having the highest outlet angle β_2=60° has the highest efficiency, 3-D CFD confirming qualitatively the quasi-3-D predictions as depicted in Figure 21.

6. Optimum number of blades

All CFD and quasi-3-D simulations and their results presented until now use the sections pitch-chord-ratio of the reference fan. However, this might be not the optimum number of blades for reaching the desired performance parameters.

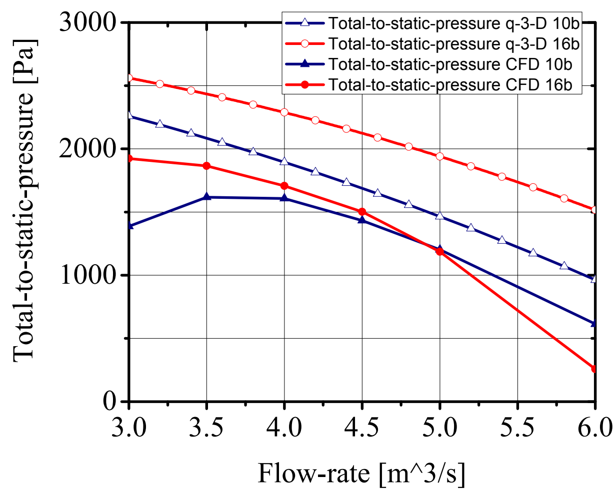

Figure 22 QUASI-3D AND FULL 3-D CFD TOTAL-TO-STATIC PRESSURE OF A FAN WITH 10 AND 16 BLADES

For investigating the optimum number of blades we picked up one of the previously investigated designs having β_2=30° and a Q_d of 600 % (Figure 22 and Figure 23). A sufficient high Re-Number of 400000 was set for all radii according to the inlet relative velocity w_∞. In this way the length of the airfoils is set. In this contribution the total-to-static pressure Δp_{t-s} and efficiency η_{t-s} are the key performance parameters, the pitch-chord-ratio influence upon them at the middle fan radius will be investigated. At the middle radius a pitch-chord-ratio of 0.65

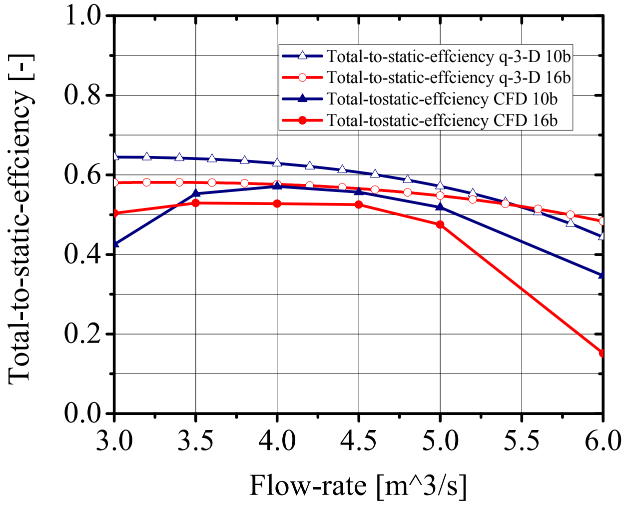

Figure 23 QUASI-3D AND FULL 3-D CFD TOTAL-TO-STATIC EFFICIENCY OF A FAN WITH 10 AND 16 BLADES

for a "high pressure design" (16 blades) was chosen as depicted in Figure 22. For the "high efficiency design" a pitch-chord-ratio of 1 (10 blades) was chosen as illustrated in Figure 23.
As pointed in Figure 22 the quasi-3-D prediction of the pressure with respect to the number of blades is reliable in terms of qualitative agreement until 4.5 [m^3/s]. The falling of the pressure of the 16 blades-design RANS simulation under the one with 10 blades is obvious owing to the higher viscous losses.

The qualitative agreement between the 3-D CFD computed efficiency and the quasi-3-D solution is pointed in Figure 23. The blade spacing quasi-3-D efficiency predictions are confirmed by a good qualitative agreement in Figure 23. The 10 blades design has a higher efficiency than the one with 16 blades and has less pressure at the design point (4[m^3 s^{-1}]).

7. Final design

In this section the performances of the impeller design with 10 blades is compared with the reference impeller. The pressure increase of the reference is very well met by the new design as illustrated in Figure 24. The efficiency is increased by the new design with almost 10% all over the flow range and the maximum flow-range is increased by the new fan. The new designed fan met all requirements set at the beginning of the process; its efficiency was improved at the working point with 10%.

CONCLUSIONS

A new framework of designing axial flow fans using thin-cambered airfoils of arbitrary shape is presented in this publication. The analytical approach has shown how the free-vortex distribution can be specified at any flow-rate and what the expected performances are. For generating the blade sections an original mean-line design procedure was developed. The deflection angle and its impact on the fan performance has been investigated by using new quasi-3-D simulations procedure. The inviscid deflection and hence the inviscid cascade loss predicts an substantial amount of the total 3-D deflections as depicted first in the analytical and quasi-3-D section and then in the comparison between quasi-3-D and 3-D CFD simulations section. Also the quasi-3-D approach confirms qualitatively the effects of blade number on the performances of the axial fans as validated by 3-D CFD simulations.

The computational effort in the design process using the quasi-3-D method is very small in terms of time (about 10 seconds for the complete flow-range on a 3GHz PC) while compared to the same number of full CFD simulations.

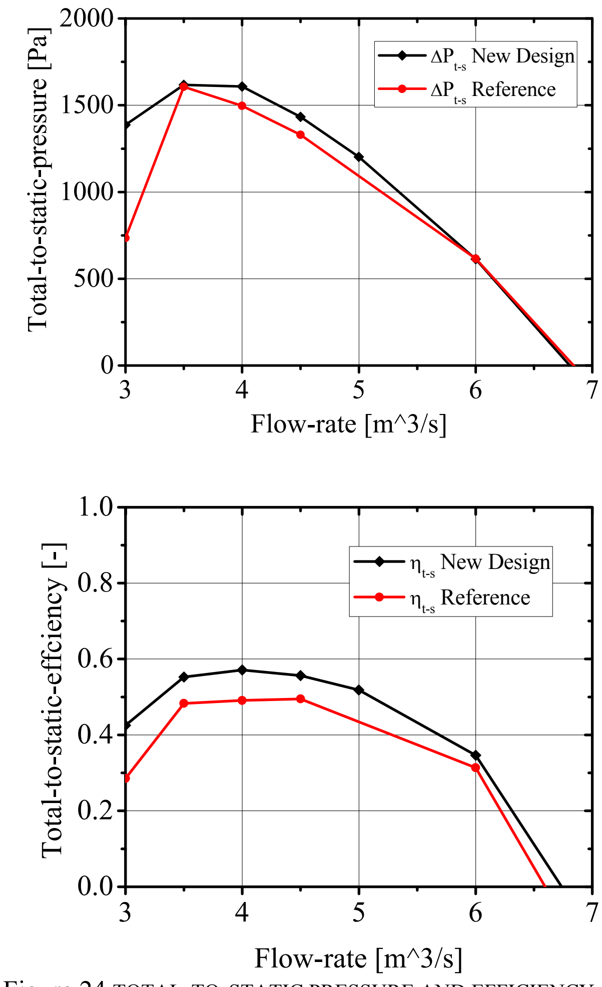

Figure 24 TOTAL-TO-STATIC PRESSURE AND EFFICIENCY OF THE REFERENCE AND OF THE NEW DESIGN

NOMENCLATURE

Latin symbols

c	[m s^{-1}]	absolute velocity
c_{md}	[m s^{-1}]	meridional design velocity
C_l	[-]	lift coefficient
d	[m]	diameter
i	[-]	complex number
l	[m]	chord length
m	[%]	NACA airfoils camber
n	[min^{-1}]	speed
n_q	[min^{-1}]	specific speed
p	[Pa]	pressure
p	[%]	NACA airfoil camber position
P	[W]	Power
Q	[m^3 s^{-1}]	flow rate
r	[m]	radius
R	[-]	Reaction
Re	[-]	Reynolds number
t	[-]	cascade pitch
[t/l]	[-]	pitch-chord-ratio
u	[-]	non-dimensional x velocity
U	[m s^{-1}]	peripheral velocity
v	[-]	non dimensional y velocity
v_∞	[m s^{-1}]	velocity
w	[m s^{-1}]	relative velocity
z	[-]	number of blades

Greek symbols

α	[rad]	incidence angle,
ß	[rad]	blade angle/flow angle
δ	[rad]	deviation angle $\delta = \beta_{2p} - \beta_2$
Δ	[-]	variation of a quantity
Δβ	[rad]	blade turning angle
Γ	[m^2 s^{-1}]	vortex strength (panel)
λ	[rad]	stagger angle
θ	[rad]	camber angle
η	[−]	efficiency
ν	[m² s^{-1}]	kinematic viscosity of air
ζ	[rad]	panel angle
ρ	[kg m^{-3}]	density
σ	[-]	cascade solidity

Subscripts and Superscripts

1	at the impeller inlet
2	at the impeller exit
d	design
D	design
m	meridional
P	potential
t	total
s	static
t-s	total-to-static
imp	impeller
t (tip)	referring to tip
h (hub)	referring to hub

REFERENCES

[1] Lewis, R. I., 2004. “Turbomachinery performance analysis”. Elsevier.

[2] Martensen E., 1959. “Berechnung der Druckverteilung an Gitterprofilen in ebener Potentialströmung mit einer Fredholmschen Integralgleichung”. Arch. Rat. Mech., Anal., 3, pp.135-170.

[3] Katz J., Plotkin A., 1991. “Low-Speed Aerodynamics”, Mc-Graw-Hill.

[4] Weinig F., 1935. “Die Strömung um die Schaufeln von Turbomaschinen”. J.A. Barth, Leipzig.

[5] Scholz N., 1965. „Aerodynamik der Schaufelgitter“. K. Braun Verlag, Karlsruhe.

[6] Eck, B., 1972. ”Ventilatoren – Entwurf und Betrieb der Radial-, Axial- und Querstromventilatoren“. 5. Auflage, Springer-Verlag, Berlin.

[7] Carolus, Th., ”Ventilatoren”. Teubner-Verlag ,2003

[8] Epple Ph., Karic, B., Ilíc, Č, Becker, S., Durst, F and Delgado. A, 2009. “Design of radial impellers: a combined extended analytical and numerical method”, Proc. IMechE, Part C: J. Mechanical Engineering Science, 223, pp. 901-917.

[9] Miclea-Bleiziffer M., Epple Ph., Delgado A., 2010. “Inverse analytical and computational design method applied to a low pressure axial fan”, Proceedings of the ASME IMECE 2010, paper IMECE2010-38614.

[10] Pascu M., Miclea M., Epple Ph., 2009. “Analytical and numerical investigation of the optimum pressure distribution along a low pressure axial fan blades”, Proc. IMechE Vol.223 Part C: J. Mechanical Engineering Science, pp. 643-658.

[11] Budugur Lakshminarayana, 1996. “Fluid Dynamics and Heat Transfer of Turbomachinery”. John Wiley & Sons.

[12] Eckert, B. und Schnell, E., 1972.: “Axialkompressoren und Radialkompressoren, Anwendung – Theorie – Berechnung“. Springer – Verlag, Berlin.

[13] Bohl W. ,2007. ”Strömungsmaschinen Vol.1 & Vol.2”, Vogel Verlag.

[14] Menter, F.R., 1993. “Zonal two-equation k-ω turbulence models for aerodynamic flows”. AIAA Paper 96-2906.

[15] J. E. Bardina, P. G. Huang, T. J. Coakley, 1998. “TurbuIence ModeIing Validation Study”. NASA Ames Research Center September.

[16] DIN Norm 24-163 Taschenbuch, Bueth Verlag, 1998

[17] Ansys Inc., November 2009. ANSYS CFX-Solver Modeling Guide. Release V12.1

[18] Ansys Inc., April 2009. ANSYS TurboGrid User's Guide V12.0.

[19] Ferziger, Peric, 2002.“Computational Methods for Fluid dynamics “. Springer.

[20] Hirsch, C, 2007. “Numerical Computation of Internal and External Flows”. Volume 1: Fundamentals of Computational Fluid Dynamics, Second edition, Elsevier.

[21] Dixon S.L., 1998. “Fluid Mechanics and Thermodynamics of Turbomachinery”. Fourth Edition, Butterworth-Heinemann.

[22] Schlichting H., Scholz N., 1951. “Uber die theoretische Berechnung der Strömungsverluste eines ebenen Schaufelgitters“. Ingenieur-Archiv, Band XIX, pp.42-65.

[23] Wallis R.A., 1983. “Axial flow fans and ducts”. John Wiley & Sons.

[24] Sorensen D.N., Sorensen J.N., June 2000. “Toward Improved Rotor-Only Axial Fans—Part I: A Numerically Efficient Aerodynamic Model for Arbitrary Vortex Flow”. Journal of Fluids Engineering, Vol.122, , pp.318-323.

[25] Bommes L., Fricke J., Grundmann R.,2003. “Ventilatoren”,Vulkan-Verlag Essen.

